



Universiteit
Leiden

The Netherlands

A culture medium based approach to optimize the stratum corneum barrier of human skin equivalents

Helder, R.W.J.

Citation

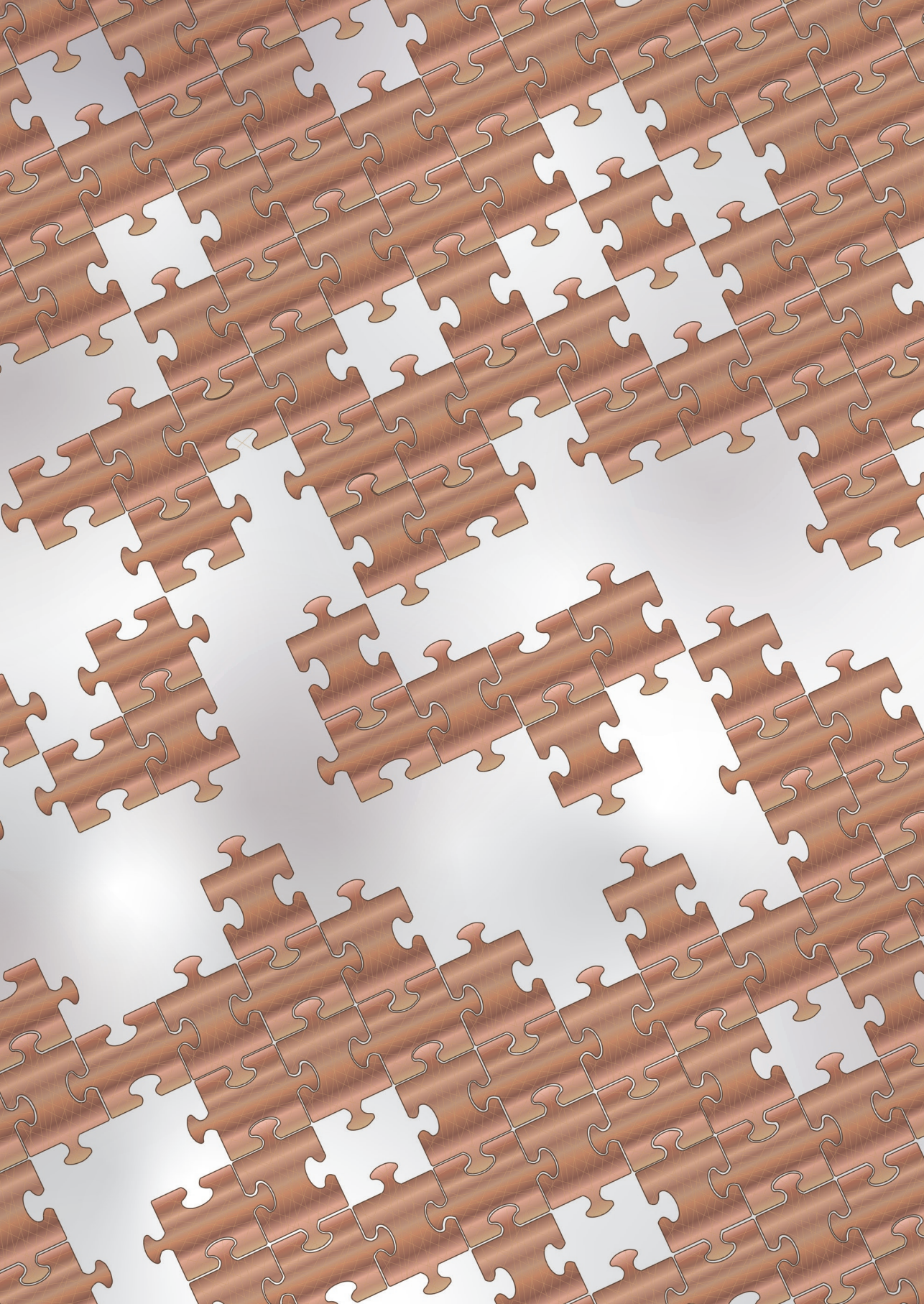
Helder, R. W. J. (2022, December 7). *A culture medium based approach to optimize the stratum corneum barrier of human skin equivalents*. Retrieved from <https://hdl.handle.net/1887/3497370>

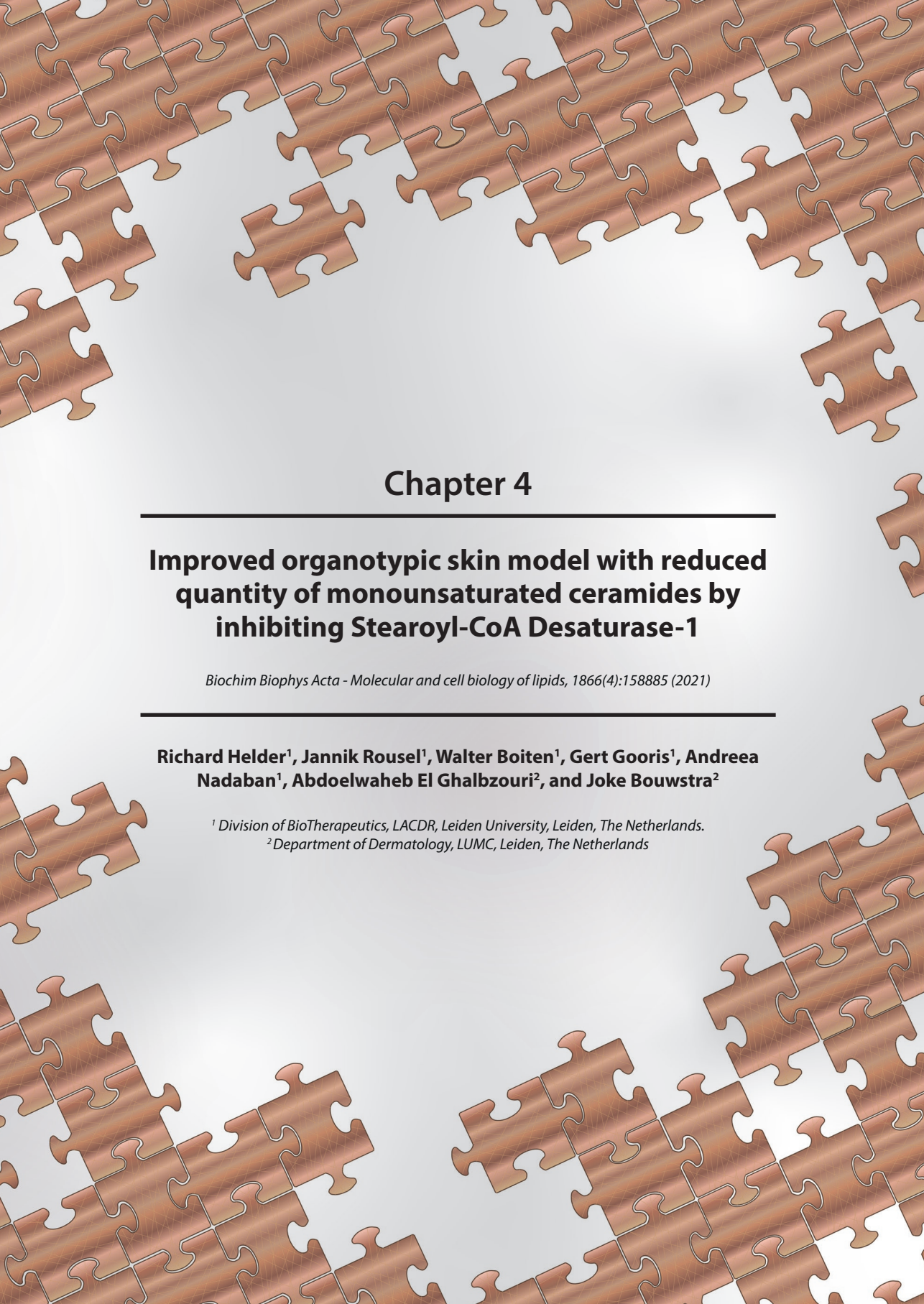
Version: Publisher's Version

License: [Licence agreement concerning inclusion of doctoral thesis in the Institutional Repository of the University of Leiden](#)

Downloaded from: <https://hdl.handle.net/1887/3497370>

Note: To cite this publication please use the final published version (if applicable).





Chapter 4

Improved organotypic skin model with reduced quantity of monounsaturated ceramides by inhibiting Stearoyl-CoA Desaturase-1

Biochim Biophys Acta - Molecular and cell biology of lipids, 1866(4):158885 (2021)

Richard Helder¹, Jannik Rousel¹, Walter Boiten¹, Gert Gooris¹, Andreea Nadaban¹, Abdoelwaheb El Ghalbzouri², and Joke Bouwstra²

¹ Division of BioTherapeutics, LACDR, Leiden University, Leiden, The Netherlands.

² Department of Dermatology, LUMC, Leiden, The Netherlands

Abstract

Full thickness models (FTM) are 3D *in vitro* skin cultures that resemble the native human skin (NHS) to a great extent. However, the barrier function of these skin models is reduced. The skin barrier is located in the stratum corneum (SC) and consists of corneocytes embedded in a lipid matrix. In this matrix, deviations in the composition of the FTMs lipid matrix may contribute to the impaired skin barrier when compared to NHS. One of the most abundant changes in lipid composition is an increase in monounsaturated lipids for which Stearoyl-CoA desaturase-1 (SCD-1) is responsible. To improve the SC lipid composition, we reduced SCD-1 activity during the generation of the FTMs. These FTMs were subsequently assessed on all major aspects, including epidermal homeostasis, lipid composition, lipid organization, and barrier functionality. We demonstrate that SCD-1 inhibition was successful and resulted in FTMs that better mimic the lipid composition of FTMs to NHS by a significant reduction in monounsaturated lipids. In conclusion, this study demonstrates an effective approach to normalize SC monounsaturated lipid concentration and may be a valuable tool in further optimizing the FTMs in future studies.

Keywords: Ceramide, Monounsaturatation, Skin, Stearoyl-CoA desaturase-1, Stratum corneum.

1. Introduction

Full thickness skin models (FTMs) are *in vitro* skin models that mimic native human skin (NHS) in many aspects and serve as a valuable tool to unravel biological processes in healthy and diseased skin [1]. In addition, FTMs serve as an excellent tool for the prediction of toxicity screenings and diffusion of novel compounds as an alternative for animal experiments [1-4]. However, the most important drawback is the reduced barrier function of the FTMs [5-8]. This limits the use of FTMs in the prediction of novel pharmaceutical compounds on their diffusion across the skin. Therefore, there is an urgent need for a new generation of FTMs that mimic the NHS barrier properties more closely. To improve the skin barrier of the FTMs, normalization of the stratum corneum (SC) lipid composition is considered to be crucial [9-11].

The outside-in NHS barrier is primarily located in the SC, which consists of corneocytes embedded in a lipid matrix [12]. In this lipid matrix, three main lipid classes are present: cholesterol, free fatty acids (FFAs), and ceramides (CERs). The CERs are the most complex of these lipids and over 16 subclasses have been identified [13-15]. In addition to different subclasses, each subclass has a broad distribution in their total chain length as well (sphingoid base + acyl chain) [16, 17]. Although less variety in subclasses, the FFAs also have a broad distribution of chain length. Together with cholesterol, these lipids can organize themselves into two lamellar phases, the short periodicity phase (SPP) with a repeat distance of around 6 nm and the long periodicity phase (LPP) with a repeat distance of approximately 13 nm [18, 19]. Within the lamellae, the lipids can adopt a very dense (orthorhombic), a less dense (hexagonal) packing or even a fluid phase. The lipid organization is depicted schematically in Fig S1 and the molecular structure of the various CER subclasses are described in Fig S2.

Differences in lipid composition and organization have been reported between the FTMs and NHS [16, 20]. One of the most prevalent difference is a high level of monounsaturated CERs (muCERs) and monounsaturated FFAs (muFFAs). Besides this major difference, other differences are observed as well: 1) an altered CER subclass profile, 2) a strong reduction in the FFA amount, 3) a reduction in the mean chain length (MCL) of the CERs and FFAs [5, 16, 21]. These changes in lipid composition lead to changes in the lipid organization. The most predominant ones include a shorter repeat distance of the LPP, the absence of the SPP and a less dense lipid packing: lipids adopt mainly a less dense hexagonal packing. Ultimately, these changes contribute to a reduced barrier function in the FTMs [16, 20].

The aim in this study was to improve the lipid composition by reducing the level of muCERs and muFFAs in our in-house FTM model. This in-house model displays the alteration in lipid composition and organization as described above, such as an increase in monounsaturation of the lipids [16]. A possible underlying factor for this is the enzyme stearoyl-CoA desaturase-1 (SCD-1). Studies have reported that this enzyme is overexpressed and is also present in the

suprabasal layers, whereas in NHS, SCD-1 is mainly expressed in the basal layer [16, 21].

SCD-1 serves as a catalyst for creating a double bond at the $\Delta 9$ carbon in saturated FFAs (C16:0 and C18:0) to convert them in their monounsaturated counterparts (C16:1, and C18:1), respectively [22]. Subsequently, these saturated FFAs (saFFAs) and muFFAs are elongated by a group of elongases referred to as ELOVLs and finally incorporated into the SC lipid matrix [23]. Next, these (mu)FFAs are also building blocks for CERs and are linked to a sphingoid base by the group of ceramide synthases leading to the more complex CER subclasses [24-26]. However, this means that a higher quantity of both CERs and FFAs that contain monounsaturated bonds in their acyl chains are synthesized. These muCERs and muFFAs are key factors that contributes to the formation of a less dense hexagonal organization [9]. To reduce the level of monounsaturation in the SC lipids, the culture medium of our in-house developed FTM was supplemented with an SCD-1 inhibitor to normalize the lipid monounsaturation.

After generation of FTMs, the lipid composition was analyzed and a drastic reduction in the amount of muCERs and muFFAs were observed. This demonstrates that the SCD-1 inhibitor successfully inhibited the SCD-1 activity. In addition, changes were observed in the lipid synthesis, such as the increase in CER[dS] and the overall reduction in CER(EO) subclasses.

2. Materials and Methods

Methods performed in this study are briefly described below. A more detailed description can be found in the supplemental materials and methods (Supplementary Methods).

2.1 Generation of the full thickness models

Prior to the SCD-1 study, two concentrations of SCD-1 inhibitor were tested: 45 nM and 450 nM. However, the 450 nM did not result in viable FTMs, therefore this study was performed with 45 nM as concentration for the SCD-1 inhibitor. To study the effects of SCD-1 inhibition, all studies were performed in triplicate using keratinocytes from three female donors (3 Caucasian female skin donors aged between 18-26, cell isolation is described in Supp. Methods 1). Two out of three originating NHS keratinocyte donor samples were also used as a control in the following subsequent studies (liquid-chromatography-mass spectrometry (LC-MS), quantitative polymerase chain reaction (qPCR), small angle X-ray diffraction (SAXD)). Due to limit of sample material the third control was from an additional donor. Using each donor, the FTMs were generated in triplicate. First, the dermal compartment was prepared as reported in detail previously [5, 27]. To this end, rattail-collagen was populated with fibroblasts (4×10^4 fibroblasts/ml) as described before [5]. After 7 days of culturing the dermal compartment, keratinocytes (2.5×10^5 cells) were seeded onto each dermal compartment and subsequently cultured for another four days under submerged

conditions. Then the FTMs were lifted to the air-liquid interface and the SCD-1 inhibitor was supplemented to the culture medium. The FTM conditions were: 1) FTM_{CONTROL}, that contained normal culture medium as described elsewhere [20], 2) FTM_{SCD-1} that contained in addition to the normal culture medium, 45 nM of SCD-1 inhibitor AB142089 (Sigma-Aldrich, Zwijndrecht, the Netherlands) dissolved in 0.05% DMSO of the culture medium (v/v), 3) FTM_{DMSO} supplemented with 0.05% DMSO in the medium was cultured to serve as a second control. The results obtained in this study for FTM_{DMSO} and the FTM_{CONTROL} were similar in all features, therefore, the FTM_{DMSO} are not shown in the result section. The FTMs were cultured air exposed for a period of 14-17 days and medium was refreshed twice a week with freshly prepared supplements [27, 28]. Subsequently, the SC was removed from the viable epidermis by trypsin digestion and used for analysis (Supp. Methods 1.1).

2.2. Analysis of the FTMs

To examine the effects of the SCD-1 inhibitor on the various characteristics of the FTMs, the following analyses were performed: immunohistochemistry (Supp. Methods 1.2), LC-MS (in Supp. Methods 1.3), qPCR (Supp. Methods 1.4), SAXD (in Supp. Methods 1.5), Fourier transformed infrared spectroscopy (FTIR, in Supp. Methods 1.6), and trans epidermal water loss (TEWL, in Supp. Methods 1.7).

2.3. Statistical Analysis

Statistical analysis was performed in GraphPad 7. For statistical analysis, an unpaired t-test was performed between the FTM_{CONTROL} and FTM_{SCD-1}. To compare the FTM_{CONTROL} against NHS, an unpaired t-test was used. Significant differences are indicated by * for p<0.05, ** for p<0.01, and *** for p<0.001.

3. Results

3.1. Supplementation of the SCD-1 inhibitor led to minor changes in the epidermal homeostasis but drastically increased SCD-1 protein expression

Before the initial study on FTMs, a small pilot was performed to determine the effects of the SCD-1 inhibitor in two different concentrations; 45 nM and 450 nM. The concentration of 45 nM is based on the reported IC₅₀ of AB142089, which was 4.5 nM [21]. In addition to an 10 times increase, that would already demonstrate an effect without causing toxicity to the FTMs, we also wanted to include a higher concentration of the inhibitor (450 nM). This was initiated due to the high percentage of monounsaturations in the lipids of FTMs and to determine whether it would be more beneficial. However, the inhibitor concentration of 450 nM did not lead to a viable FTM (Fig S2). Therefore, the study was performed with inhibitor SCD-1 concentration of 45 nM (referred to as the FTM_{SCD-1}), which was supplemented to the

culture medium.

After culturing, FTMs and NHS were investigated on basal cell proliferation, early, and late differentiation by several epidermal homeostasis proteins markers (Fig 1). Basal cell proliferation was examined by a Ki67 protein staining. As shown in Fig 1, no significant changes in Ki67 expression was observed, irrespective the condition tested. Next, the early differentiation was investigated by staining for keratin 10 (K10) (Fig 1). K10, which stains the suprabasal cell layers, showed no changes in expression, indicating a normal execution of the early differentiation program. Next the late differentiation protein involucrin was stained. This protein was similarly expressed in FTM_{CONTROL} and FTM_{SCD-1} and equally present in the stratum granulosum as well as the stratum spinosum, whereas in NHS, involucrin was restricted to the stratum granulosum (Fig 1). When examining the SCD-1 expression, a significant difference was observed: The FTM_{SCD-1} displayed a drastic increase in SCD-1 expression compared to FTM_{CONTROL}, but both displayed expression throughout the epidermis. In NHS, SCD-1 expression was less prominently present and more restricted to the basal layer (Fig 1).

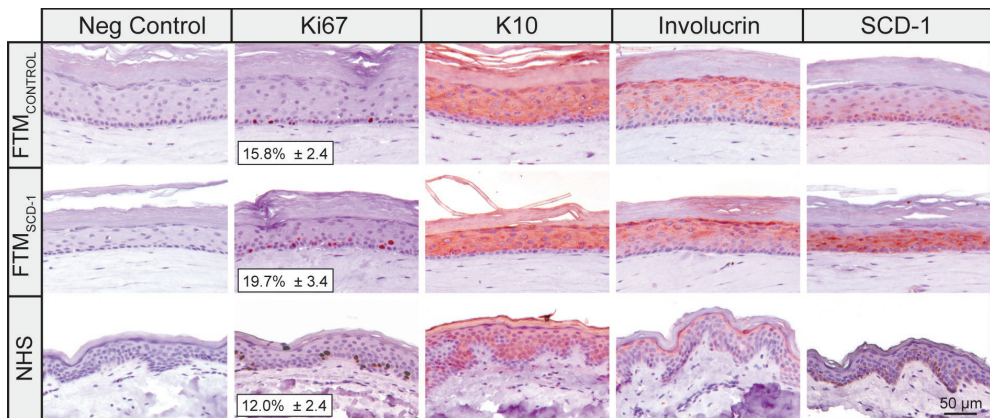


Fig 1: Different epidermal homeostasis markers and SCD-1 were examined in FTMs and NHS. Expression of protein markers in FTM_{CONTROL}, FTM_{SCD-1} and NHS from left to right: negative control, proliferation (Ki67), early differentiation (K10), late differentiation (involucrin), and lipid monounsaturase enzyme SCD-1. Ki67 proliferation index determination. Scale bar: 50 μ m.

3.2. SCD-1 Inhibition led to reduction of monounsaturated CER subclasses

To determine whether SCD-1 inhibition led to changes in the SC lipid composition, the CER profile in FTMs and NHS was examined. First, the extracted amount of SC lipids was determined (Fig 2a). The amount of extracted lipids was similar between FTMs, but was significantly increased in NHS compared to the FTMs. After the lipid extraction, the peaks of all CER subclasses (saCER+muCER) in the LC-MS spectrum were integrated, processed and converted to CER amounts in nmol/mg SC (Fig 2b). No differences in the total amount

of CERs in nmol/mg SC between the FTMs and NHS were observed. Next, the absolute amounts of the CER subclasses were analyzed.

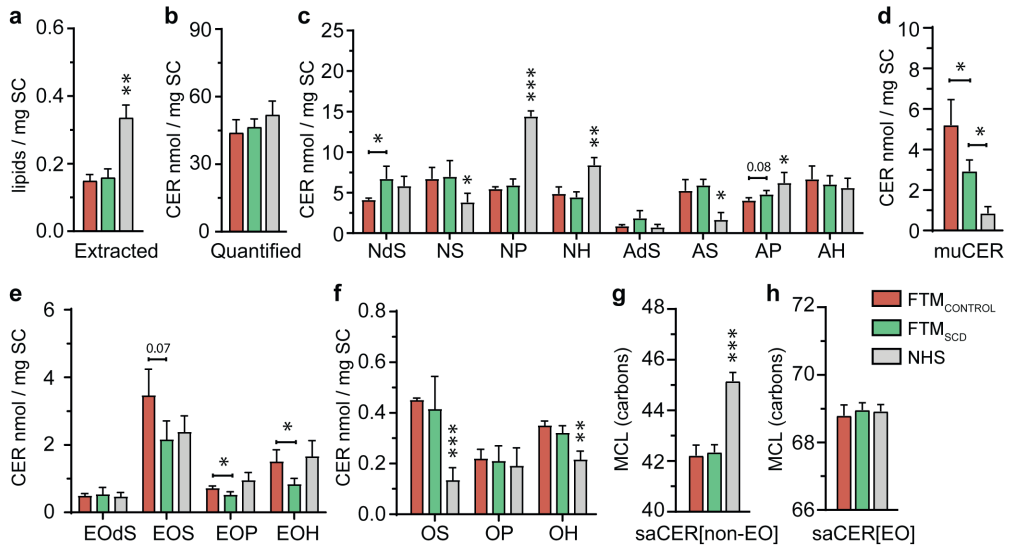


Fig 2: SCD-1 inhibition alters lipid composition by reducing the monounsaturations, reducing the CER[EO] subclasses, and by increasing the CER[dS] fraction. During sample preparation, (a) the amount of extracted lipids was determined. (b) The total amount of CERs (saCER+muCER) in nmol/mg SC. (c) The subclasses of the CER[non-EO] (saCER+muCER). (d) The total amount of muCER[non-EO] (muCERs in nmol/mg SC). (e) Subclasses in CER[EO] (saCER+muCER). (f) Subclasses in CER[O] (saCER+muCER). The mean chain lengths for (g) saCER[non-EO] and (h) CER[EO] main peak (saCER[EO-18:2]+muCER[EO-18:1]). For statistical analysis, an unpaired t-test was performed between the FTM_{CONTROL} and FTM_{SCD-1}. After, to compare the FTM_{CONTROL} and NHS, an unpaired t-test was used. Significant differences are indicated by * for p<0.05, ** for p<0.01, and *** for p<0.001.

3.2.1. Quantified CER subclass composition

The individual subclasses of CER[non-EO], CER[EO], and CER[O] were plotted in absolute amounts (Fig 2c, 2e, 2f, respectively). Individual analysis of the quantified subclasses of CER[non-EO] revealed a similar subclass profile after SCD-1 inhibition compared to FTM_{CONTROL}, except for an increased amount of CER[dS] subclass in FTMS_{CD-1}. Compared to NHS, in both FTM_{CONTROL} and FTM_{SCD-1} an altered amount of CER [NS], [AS], [NH], [NP] and [NH] subclasses was observed. More drastic changes were observed when examining the amount of muCERs after SCD-1 inhibition (Fig 2d). This demonstrated that the SCD-1 inhibitor successfully reduced the amount of muCERs to a level more closely to that in NHS.

In addition to the CER[non-EO], the CER[EO] subclasses were also quantified (Fig 2e). The total amount of CER[EO] was reduced in FTM_{SCD-1}, this was mainly caused by the reduction in CER[EOS] (p=0.07) and a significant reduction in CER[EOP] and CER[EOH] subclasses. To

study the underlying factor of this reduction, the individual monounsaturated and saturated subclasses of CER[EO] with either oleic (C18:1) or linoleic (C18:2) acid chain were analyzed (Fig S4). This displayed that it was not one individual CER[EO] subset that was reduced, but all subsets were reduced. This reduction was most prevalent in the CER[EOS], where the combined amount of muCER[EO-18:1]/ saCER[EO-18:2] was decreased (Fig S4a, $p=0.06$). Similar results were observed for the muCER[EO-18:2] (Fig S4b, $p=0.11$) and saCER[EO-18:1] (Fig S4c, $p=0.07$).

Next, to determine whether the decrease in amount of CER[EO] was due to a change in the CER[O] content as these have a common synthetic pathway, the amount of CER[O] (saCER+muCER) was determined (Fig 2f). The amount of CER[O] was similar between the FTM conditions tested. However, when studying the saCER[O] and muCER[O] composition separately (Fig S5), an increase (but not significant) in subclasses of saCER[O] in the FTM_{SCD-1} was observed more comparable to NHS, although NHS still has significantly higher amount of saCER[O].

Another important aspect for the barrier is the mean chain length (MCL) of the lipids. This was determined for both saCER[non-EO] (Fig 2g) and the main CER[EO] subclass (Fig 2h) subclasses. Inhibition of SCD-1 did not have an impact on the MCL of the CER[non-EO]; The MCL was still shorter compared to that of NHS [21, 29]. The MCL of CER[EO] were comparable between the FTMs and NHS groups and did not change in the FTM_{SCD-1} compared to FTM. In addition, to determine whether some CER chain lengths were more abundantly present in FTM_{SCD-1} than in FTM, the chain length distribution was determined in absolute and relative amounts (Fig S6). The absolute chain length distribution displayed some minor but significant differences between the FTM conditions for CER[non-EO] subclasses. The amount of CERs with a chain length of C36, C38, C44 and C46 were increased in FTM_{SCD-1} compared to FTM_{CONTROL}. When comparing the CER chain length profile of the FTMs to NHS, there is still a large amount of CER of <C42 present in FTMs, where in NHS most CERs contain >C42. Next, the absolute CER[EO] chain length distribution was investigated. For most of the chain lengths (with the exception of C68, and C74) the chain length distribution of CER[EO] in FTM_{SCD-1} mimicked closely the distribution in NHS. However, this was mainly due to the decreased total amount of CER[EO] in FTM_{SCD-1}. When examining the relative chain length distribution, hardly no difference in chain length distribution was present between FTM_{SCD-1} and FTM_{CONTROL}.

3.2.2. Relative CER subclass composition

In order to relate changes in lipid composition to lipid organization, relative amounts of CER subclasses are important. The composition of the relative amounts of CER[non-EO] and CER[EO] are reported in Fig S7 and Fig S8, respectively. Briefly, the CER changes reported in Fig 2 became more prominent when determining the percentage of CER subclasses.

Such as the higher percentage of CER[dS] subclass and a significant reduction of most of the CER[EO] subclasses: CER[EOS], [EOH], and [EOP]. Finally, when examining the level of CER[non-EO] monounsaturations, the difference was more abundant ($p=0.007$ vs $p=0.05$) when the amount of CERs (%) was calculated for each FTM donor.

3.3. SCD-1 inhibition reduced muFFA in FTMs

3.3.1 Quantified FFA analysis

The total amount of FFA in FTMs (saFFA+muFFA) did not change upon SCD-1 inhibition (Fig 3a). Inhibition of SCD-1 did not change the chain length distribution of saFFA either (Fig 3b). The amount of all saFFA irrespective of their chain length was strongly reduced compared to NHS as observed in earlier studies [21, 29]. Next, the muFFA profile was determined (Fig 3c). Inhibition of SCD-1 reduced the amount of muFFA C16:1, C18:1, and C24:1 in the FTM_{SCD-1} compared to FTM_{CONTROL}. This was also reflected in the total amount of muFFA (Fig 3d) and resulted in a reduced percentage of muFFA in FTM_{SCD-1}, as shown in Fig 3e. This percentage indicates that the muFFA content in FTMs were higher than in NHS and SCD-1 inhibition was a valuable approach to reduce the muFFA content to mimic more closely the level in NHS. In addition, the FFA MCL was determined (Fig 3f), SCD-1 inhibition did not affect the MCL.

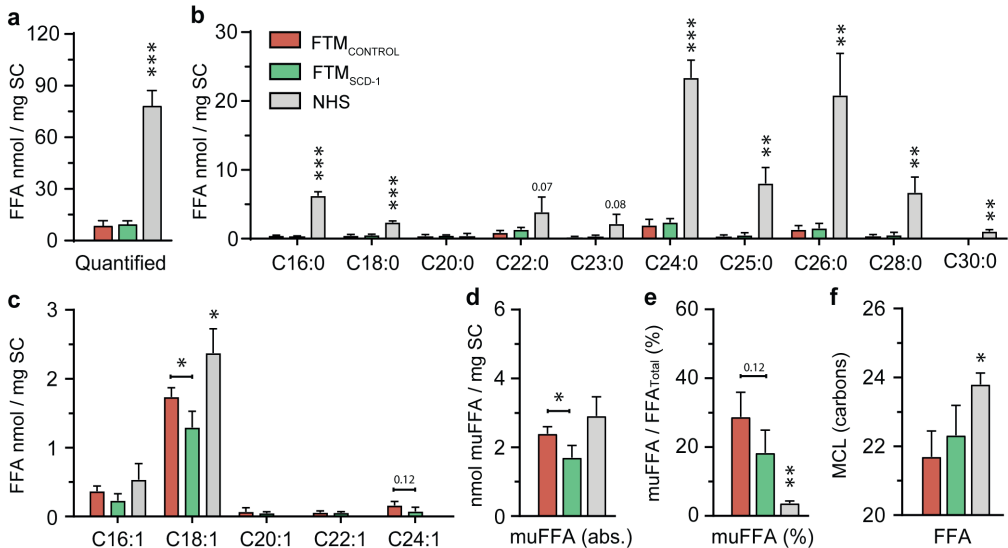


Fig 3: SCD-1 inhibition led to a reduction in the amount of monounsaturated FFAs. (a) Amount of FFA in nmol / mg SC (b) Absolute saFFAs as function of chain length; (c) Absolute amount of muFFAs as function of chain length; (d) Absolute amount of muFFA in nmol / mg SC; (e) The percentage of muFFA; (f) the saFFA MCL. For statistical analysis, an unpaired t-test was performed between the FTM_{CONTROL} and FTM_{SCD-1}. To determine whether significant differences were observed between FTM_{CONTROL} and NHS, an unpaired t-test was used. Significant differences are indicated by * for $p<0.05$, ** for $p<0.01$, and *** for $p<0.001$.

3.3.2 Relative FFA analysis

In order to relate changes in FFA composition to lipid organization, percentages of FFA subclasses were also calculated (Fig S9). These results demonstrate that especially long chain FFAs (>C24) were reduced and the short chain FFAs (<C22) were increased in FTMs compared to NHS. Although no significant effects were observed by SCD-1 inhibition on the MCL of the lipids, the muFFA content was significantly reduced in the FTM_{SCD-1}.

3.4. Effect of the SCD-1 inhibition on the lipid synthesis genes

To obtain information on the underlying factors that might explain the lipid composition changes after SCD-1 inhibition, several genes that are involved in lipid synthesis, elongation of FFA, and the CER synthesis were investigated (Fig 4).

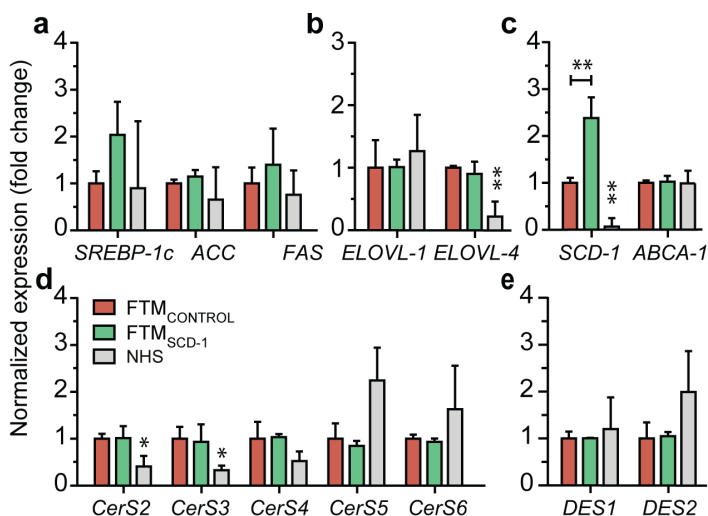


Fig 4: Minor changes in the expression of genes involved in lipid synthesis, lipid processing, or CER synthesis after SCD-1 inhibition. Lipid synthesis genes investigated for FTM_{CONTROL}, FTM_{SCD-1}, and NHS. (a) Lipid synthesis genes SREBP-1c, ACC, and FAS. (b) Lipid elongases ELOVL-1 and ELOVL-4. (c) Lipid desaturase SCD-1 and LXR downstream target ABCA1. (d) CER synthases 2-6, and (e) CER processing enzymes DES1 and DES2. For statistical analysis, an unpaired t-test was performed between the FTM_{CONTROL} and FTM_{SCD-1}. To compare the FTM_{CONTROL} and NHS, an unpaired t-test was used. Significant differences are indicated by * for p<0.05, ** for p<0.01.

For the lipid processing genes (SREBP-1c, ACC, and FAS), no difference in gene expression between the FTM_{SCD-1} and FTM_{CONTROL} was observed. This was also observed for the lipid elongation genes ELOVL-1 and ELOVL-4 (Fig 4b). However, an increased ELOVL-4 expression was observed in FTMs when compared to NHS. The next gene that was investigated was SCD-1 (Fig 4c). This gene was drastically increased in the FTM_{SCD-1} when compared to the FTM_{CONTROL}. In addition, the FTM_{CONTROL} already expressed significantly higher SCD-

1 compared to NHS. To examine whether this increase was driven by LXR activation, ABCA1 gene expression (Fig 4c) was investigated. However, no change in this gene was observed, excluding LXR activation as underlying factor. Next, the CER synthesis genes were investigated. No differences in expression of the Ceramide Synthases (CerS) were observed between FTMs (Fig 4d). However, a higher expression for CerS2 and CerS3 were observed in FTMs compared to NHS. Finally, the gene expression of the enzymes that play a role in the head group synthesis were examined. DES1 and DES2 convert the CER[dS] subclass to CER[S] and CER[P], respectively. No differences were observed for these genes in FTM_{CONTROL} and FTM_{SCD-1}. However, DES2 was slightly decreased in FTMs compared to NHS.

3.5. Effect of SCD-1 inhibition on the lipid organization and TEWL

To investigate whether the changes in lipid composition affected lipid organization and subsequently SC barrier, the lipid organization and SC barrier function were examined (Fig 5). For comparison all presented data were measured at 24°C.

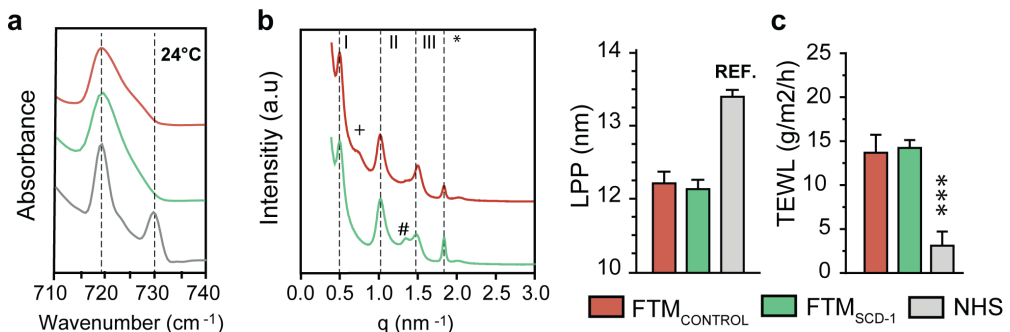


Fig 5: SCD-1 inhibition does not change lipid organizations or lipid permeation. The lipid organization was analyzed for the FTMs and NHS at 24°C (a) the lateral organization by displaying the rocking region and (b) X-ray diffraction profile for FTMs and the LPP repeat distance. Diffraction order of the LPP is indicated by I, II, and III. The cholesterol phase is indicated by the asterisk (*). Unknown phases are indicated by + and #. The repeat distance is provided in the bar plot, with NHS as a reference [18]. (c) The TEWL values are plotted in a bar plot. For statistical analysis, an unpaired t-test was performed between the FTM_{CONTROL} and FTM_{SCD-1}. After, to compare the FTM_{CONTROL} vs NHS, an unpaired t-test was used. Significant differences are indicated by *** for p < 0.001.

FTIR was used to determine the lateral organization of the lipids (Fig 5a). We present the rocking vibrations at 24°C, the temperature at which the TEWL measurement was performed (see below). The high peak intensity of the vibration located at 719 cm⁻¹ together with a small shoulder located at 730 cm⁻¹ in the FTIR spectrum of FTM_{CONTROL} indicates that most lipids adopt a hexagonal packing. A similar rocking pattern was observed for FTM_{SCD-1}. In the spectrum of NHS, the intensity of the vibrations at 730 cm⁻¹ was much stronger indicating that a higher fraction of lipids adopt to an orthorhombic organization. This demonstrates a less dense lipid organization in the FTMs compared to that in NHS.

Next, we determined the lamellar organization using X-ray diffraction (Fig 5), the peak positions, indicated by I, II and III refer to the various orders of a lamellar phase with a repeat distance of 12.1 nm and 12.2 nm for the FTM_{SCD-1} and FTM_{CONTROL}, respectively. Besides this diffraction pattern two additional small peaks were observed in the SAXD profile, indicated by + and #.

To determine whether the changes in lipid organization (FTIR and SAXD) led to a change in the barrier function of FTM_{SCD-1} compared to FTM_{CONTROL} the TEWL was measured for FTMs and NHS (Fig 5c). No differences were observed after SCD-1 inhibition in the FTMs. However, the TEWL of NHS was approximately 4.5 times lower than that of the FTM_{CONTROL}.

4. Discussion

Our aim was to improve the lipid composition and organization in the FTM model by modulating the activity of SCD-1. By inhibiting SCD-1, several modifications were observed on the lipid composition. The most important modification was the reduction in the amount of muCERs and muFFAs in the SC of the FTM_{SCD-1}, which resembles the lipid composition in NHS more closely. Another important finding was that the quantity of lipids remained similar after SCD-1 inhibition, which indicates that the total amount of lipids synthesized was unaffected by the SCD-1 inhibition and thus the synthesis of saCERs and saFFAs was increased at the expense of the monounsaturated variant. In addition, several other lipid compositional changes were observed.

First, there was a strong decrease in the amount of CER[EO] observed in the FTM_{SCD-1}. Interestingly, when displaying the individual CER[EO] subsets, both muCER[EO-18:2] and saCER[EO-18:1] are reduced, together with the main CER[EO] peak composed of two CER subclasses: muCER[EO-18:1]/saCER[EO-18:2]. This reveals that not only the muCER[EO] contributed to this reduction, but the CER[EO-18:1] as well. To understand why the CER[EO] was reduced, as a first possible underlying factor, enzymes responsible for the synthesis of CER[EO] were investigated. For this synthesis CerS3 and ELOVL4 are required [30], but the gene level for ELOVL4 and CerS3 did not change between FTM_{CONTROL} and FTM_{SCD-1}. A second possible factor is an increase in CER[O], since CER[EO] is a precursor for CER[O] [31, 32]. However, similar amounts of CER[O] were observed in the FTMs. A third explanation is a reduction in the amount of oleic acid (C18:1) for the synthesis of the CER[EO-18:1]. The amount of C18:1 was reduced in the FTM_{SCD-1} and therefore might be an underlying factor of the reduction of CER[EO-18:1]. When comparing FTMs to NHS, the amount of CER[EO] in FTMs is increased. Both CerS3 and ELOVL4 are known to play a key role in the synthesis of CER [4, 30], the increased mRNA expression of these genes in FTMs might explain why the amount of CER[EO] is higher in FTMs.

Second, we observed an increase in the absolute amount of CER[dS] in the FTM_{SCD-1} compared

to the FTM_{CONTROL}. This effect was even more prevalent when relative amounts of CERs were calculated. To investigate whether the increase in the amount of CER[dS] was due to a reduction in the CER head group synthesis genes, the CER subclass synthases DES1 and DES2 that are responsible for the conversion of CER[dS] to CER[S] and CER[P], respectively, were investigated on gene level. As both FTMs had similar mRNA level for DES1 and DES2, there is no indication that these genes are an underlying factor of the shift towards more CER[dS]. However, when observing the morphology of the FTM_{SCD-1}, the epidermis does appear thinner. Perhaps, the differentiation is performed more rapidly, giving the ceramide processing enzymes less time to convert the head groups resulting in a higher level of CER[dS]. In addition, higher levels of CER[dS] were also observed in mouse skin, which also has a very thin epidermis [33]. Indicating that the thickness of the epidermis might have an impact on the subclasses.

When studying epidermal morphology and protein expression, an interesting observation is that SCD-1 inhibition resulted in a drastic increase in SCD-1 expression on both protein and RNA level. Even with an increased expression, the SCD-1 inhibitor still inhibited the majority of the protein, since there was a significant reduction in muCERs observed. This increase in SCD-1 protein level was likely due to the necessity to maintain several crucial biological processes, such as regulating cell survival, membrane integrity, or preventing lipotoxicity in the cells [34-39].

Although the effects of SCD-1 inhibiting resulted in an improved lipid composition, the observed changes ultimately did not lead to alterations in the lateral organization and both FTMs adopted a hexagonal lipid organization. In order to advance the lipid organization of FTMs, several key-changes may be an important next step to generate FTMs with normalized barrier function: 1) Perhaps the most crucial change, is the increase in the quantity of FFAs. In NHS, the ratio between CER:FFA in this study is approximately 0.8:1, whereas the ratio in FTMs is approximately 1:0.125. Normalization of this ratio would promote the lipids to adopt an orthorhombic packing in FTMs [40]. 2) An increase in the MCL of both CERs and FFAs would enhance SC lipids to adopt an orthorhombic organization [21]. Another study demonstrated that LXR inhibition reduced the muCERs, but at the same time also an increase in chain length was observed [21]. This subsequently also led to an improved lipid organization, demonstrating the importance of targeting both the monounsaturations and lipid chain length. 3) A further reduction in the amount of muCERs and muFFAs would likely result in a higher fraction of lipids forming an orthorhombic organization as shown in previous studies [9].

SCD-1 inhibition did not alter the lamellar organization. The diffraction patterns of the FTMs revealed lamellar phases in the FTMs. Although it remains to be elucidated why the phases + and # formed, these small changes are most probably observed due to the CER subclass composition as this composition is crucial for the formation of the lamellar phases [41].

In the FTM_{SCD-1'}, the fraction of CER[EO] is reduced and the additional phase + is no longer present, which could indicate that the abundant presence of CER[EO] contributes to this peak as suggested in previous studies [42]. The phase # might be attributed to the increased amounts of CER[dS] in the FTM_{SCD-1'} since the FTM_{CONTROL} does not contain this phase.

To conclude, this study demonstrates that SCD-1 activity could be successfully reduced and that SCD-1 modulation can be a tool to lower the amount of muCERs and muFFAs in our FTM models. However, although a reduced SCD-1 activity improved the lipid composition, it did not result in an improved barrier function. This demonstrates the complexity of the lipid synthesis and the subsequent formation of the lipid organization. Nevertheless, it is important to know that the approach to reduce the monounsaturated lipids is useful, it should be combined with other targeted approaches to improve the lipid composition in order to generate the next generation of FTMs that even better mimic NHS.

5. Acknowledgements

We would like to thank the Dutch Technology Foundation TTW for their grand contribution (13151). TTW is also part of the Netherlands Organization for Scientific Research (NWO). We thank Evonik for their supply of ceramides. Last, we like to thank the DUBBLE beam line staff of station BM26 for their support and help the European synchrotron radiation facility (Grenoble, France).

References

1. Niehues, H., et al., 3D skin models for 3R research: The potential of 3D reconstructed skin models to study skin barrier function. *Exp Dermatol.*, 2018. 27(5): p. 501-511.
2. El Ghalbzouri, A., et al., Leiden reconstructed human epidermal model as a tool for the evaluation of the skin corrosion and irritation potential according to the ECVAM guidelines. *Toxicol In Vitro.*, 2008. 22(5): p. 1311–20.
3. Lilienblum, W., et al., Alternative methods to safety studies in experimental animals: role in the risk assessment of chemicals under the new European Chemicals Legislation (REACH). *Archives of Toxicology*, 2008. 82(4): p. 211-236.
4. Schäfer-Korting, M., et al., The use of reconstructed human epidermis for skin absorption testing: Results of the validation study. *Alternatives to laboratory animals: ATLA*, 2008. 36(2): p. 161-187.
5. Thakoersing, V.S., et al., Unraveling barrier properties of three different in-house human skin equivalents. *Tissue Eng Part C Methods.*, 2012. 18(1): p. 1-11.
6. Schäfer-Korting, M., et al., Reconstructed human epidermis for skin absorption testing: results of the German prevalidation study. *Altern Lab Anim.*, 2006 34: p. 283-94.
7. M., V.G., et al., Three-dimensional skin models as tools for transdermal drug delivery: challenges and limitations. *Expert Opin Drug Deliv.*, 2011 8(6): p. 705-20.
8. Flaten, G.E., et al., In vitro skin models as a tool in optimization of drug formulation. *Eur J Pharm Sci.*, 2015 30(75): p. 10-24.
9. Mojumdar, E.H., et al., Monounsaturated Fatty Acids Reduce the Barrier of Stratum Corneum Lipid Membranes by Enhancing the Formation of a Hexagonal Lateral Packing. *Langmuir*, 2014. 30(22): p. 6534-43.
10. van Smeden, J., et al., The importance of free fatty acid chain length for the skin barrier function in atopic eczema patients. *Exp Dermatol.*, 2014. 23(1): p. 45-52.
11. J., V.S. and J.A. Bouwstra, Stratum Corneum Lipids: Their Role for the Skin Barrier Function in Healthy Subjects and Atopic Dermatitis Patients. *Curr Probl Dermatol.*, 2016. 49: p. 8-26.
12. Proksch, E., J.M. Brandner, and J.M. Jensen, The skin: an indispensable barrier. *Exp Dermatol.*, 2008 17(12): p. 1063-72.
13. Motta, S., et al., Ceramide composition of the psoriatic scale. *Biochim Biophys Acta.*, 1993. 1182(2): p. 147-51.
14. Boiten, W., et al., Quantitative analysis of ceramides using a novel lipidomics approach with three dimensional response modelling. *Biochimica et Biophysica Acta (BBA) - Molecular and Cell Biology of Lipids*, 2016. 1861(11): p. 1652-1661.
15. t'Kindt, R., et al., Profiling and Characterizing Skin Ceramides Using Reversed-Phase Liquid Chromatography–Quadrupole Time-of-Flight Mass Spectrometry. *Analytical Chemistry*, 2012. 84(1): p. 403-411.
16. Thakoersing, V.S., et al., Increased Presence of Monounsaturated Fatty Acids in the Stratum Corneum of Human Skin Equivalents. *J Investig Dermatol.*, 2013. 133(1): p. 59-67.
17. van Smeden, J., et al., LC/MS analysis of stratum corneum lipids: ceramide profiling and discovery. *J Lipid Res.*, 2011. 52(6): p. 1211-21.

Chapter 4

18. Bouwstra, J.A., et al., Structural investigations of human stratum corneum by small-angle X-ray scattering. *J Invest Dermatol.*, 1991. Dec(6): p. 1005-12.
19. Boncheva, M., The physical chemistry of the stratum corneum lipids. *International journal of cosmetic science*, 2014. 36(6): p. 505-515.
20. Thakoersing, V.S., et al., Unraveling barrier properties of three different in-house human skin equivalents. *Tissue Engineering Part C: Methods*, 2011. 18(1): p. 1-11.
21. Helder, R.W.J., et al., The effects of LXR agonist T0901317 and LXR antagonist GSK2033 on morphogenesis and lipid properties in full thickness skin models. *Biochim Biophys Acta Mol Cell Biol Lipids.* , 2019. 1865.
22. Paton, C.M. and J.M. Ntambi, Biochemical and physiological function of stearoyl-CoA desaturase. *Am J Physiol Endocrinol Metab.*, 2009. 297(1): p. E28-E37.
23. Rabionet, M., K. Gorgas, and R. Sandhoff, Ceramide synthesis in the epidermis. *Biochim Biophys Acta.*, 2014. 1841(3): p. 422-434.
24. Kihara, A., Synthesis and degradation pathways, functions, and pathology of ceramides and epidermal acylceramides. *Progress in Lipid Research*, 2016. 63: p. 50–69.
25. Mizutani, Y., et al., Ceramide biosynthesis in keratinocyte and its role in skin function. *Biochimie*, 2009. 91: p. 784-790.
26. Masukawa, Y., et al., Comprehensive quantification of ceramide species in human stratum corneum. *J. Lipid Res.*, 2009. 50(8): p. 1708-19.
27. van Drongelen, V., et al., Barrier Properties of an N/TERT-Based Human Skin Equivalent. *Tissue Eng Part A.*, 2014. 20(21-22): p. 3041-9.
28. Ponec, M., et al., The Formation of Competent Barrier Lipids in Reconstructed Human Epidermis Requires the Presence of Vitamin C. *J Invest Dermatol.*, 1997. 109(3): p. 348-55.
29. Helder, R.W.J., et al., Contribution of Palmitic Acid to Epidermal Morphogenesis and Lipid Barrier Formation in Human Skin Equivalents. *Int J Mol Sci.*, 2019. 20(23).
30. Mizutani, Y., et al., Cooperative Synthesis of Ultra Long-Chain Fatty Acid and Ceramide during Keratinocyte Differentiation. *PLoS One*, 2013. 8.
31. Zheng, Y., et al., Lipoxygenases mediate the effect of essential fatty acid in skin barrier formation: A proposed role in releasing omega-hydroxyceramide for construction of the corneocyte lipid envelope. *J Biol Chem.*, 2011. 286(27): p. 24046-56.
32. Krieg, P. and G. Fürstenberger, The role of lipoxygenases in epidermis. *Biochim Biophys Acta*, 2014. 1841: p. 390–400.
33. Martins Cardoso, R., et al., Barrier lipid composition and response to plasma lipids: A direct comparison of mouse dorsal back and ear skin. *Exp Dermatol.* 2020: p. 548-555.
34. Miyazaki, M., W.C. Man, and J.M. Ntambi, Targeted disruption of stearoyl-CoA desaturase1 gene in mice causes atrophy of sebaceous and meibomian glands and depletion of wax esters in the eyelid. *J Nutr.*, 2001 131: p. 2260-8.
35. Jackowski, S., Cell cycle regulation of membrane phospholipid metabolism. *J. Biol. Chem.*, 1996. 1271: p. 20219–20222.
36. Sampath, H., et al., Skin-specific Deletion of Stearoyl-CoA Desaturase-1 Alters Skin Lipid Composition and Protects Mice from High Fat Diet-induced Obesity. *J Biol Chem.* , 2009. 284(30): p. 108

19961–19973.

37. Golfman, L.S., M. Bakovic, and D.E. Vance, Transcription of the CTP: phosphocholine cytidyltransferase alpha gene is enhanced during the S phase of the cell cycle. *J. Biol. Chem.*, 2001. 276: p. 43688–43692.
38. Miyazaki, M., W.C. Man, and J.M. Ntambi, Targeted disruption of stearoyl-CoA desaturase1 gene in mice causes atrophy of sebaceous and meibomian glands and depletion of wax esters in the eyelid. *J Nutr.*, 2001. 131: p. 2260–2268.
39. Li, L.O., E.L. Klett, and R.A. Coleman, Acyl-CoA synthesis, lipid metabolism and lipotoxicity. *Biochim Biophys Acta.*, 2010. 1801: p. 246-51.
40. Bouwstra, J.A., et al., Phase behavior of lipid mixtures based on human ceramides: coexistence of crystalline and liquid phases. *J Lipid Res.*, 2001. 42: p. 1759-70.
41. Smeden, J.v., et al., The important role of stratum corneum lipids for the cutaneous barrier function. *Biochim Biophys Acta.*, 2014. 1841: p. 295-313.
42. Groen, D., G.S. Gooris, and J.A. Bouwstra, Model membranes prepared with ceramide EOS, cholesterol and free fatty acids form a very unique lamellar phase. *Langmuir*, 2010. 26: p. 4168-75.

SUPPLEMENTARY INFORMATION

1. Supplemental material and methods

For the experiments various analysis have been performed.

1.1. Primary cell isolation and monolayer cultures

Within 24 hours of plastic surgery, the skin was processed. After cleaning the skin by removing the excess of subcutaneous fat tissue, the skin was stretched on styrofoam and the skin surface was cleaned with demi H₂O, ethanol and again with demi H₂O prior to dermatoming to a thickness of 400 µm. Subsequently, the skin was placed overnight in 2.4 U/ml dispase II (Roche, Almere, the Netherlands). After overnight incubation, the epidermis and dermis were separated and further used for the keratinocyte and fibroblast isolation as described elsewhere [1].

1.2. Stratum Corneum isolation

Isolated SC was used for the LC-MS, SAXD, FTIR and TEWL measurements. SC isolation was performed by placing dermatomed skin (in case of NHS) or the FTMs on a cotton pad soaked in an 0.1% (w/v) trypsin (Sigma Aldrich Chemie, Zwijndrecht, The Netherlands) in PBS solution. 0.1M PBS (pH 7,4) was used and consisted of NaCl (8.13g), Na₂HPO₄ (2.87g), KHPO₄ (0.20g) and KCl (0.19g) in 1L of MilliQ. The samples were placed in the fridge at 4°C overnight, subsequently, the skin was placed in an oven for 37°C for 1 hour. This allowed the SC to separate from the epidermis. The SC was washed after separation with 0.1% (w/v) trypsin inhibitor (Sigma Aldrich Chemie, Zwijndrecht, The Netherlands) in PBS and subsequently washed twice with MilliQ. After washing, the SC was air dried and stored in a dark environment under argon and over silica prior to use.

1.3. Immuno-histochemical staining and visualization

After harvesting the FTMs, tissue samples were fixed in biopsy pads soaked in 4% paraformaldehyde (Pharma B.V., Oss, the Netherlands) for 24 hours. Subsequently, the samples were dehydrated in a series of ethanol solutions before embedding in paraffin. Sections of the sample were cut at 5 µm and collected on SuperFrost®Plus slides (VWR international B.V., Leuven, Belgium). This was left overnight at 60°C in an oven. After rehydration, heat-induced antigen retrieval was performed in a citrate buffer in the water bath or autoclave depending on the primary antibody (For specification, see table 1). After cooling to room temperature, the sections were blocked with normal human serum (2%, Sanquin, Leiden, The Netherlands). Subsequently, the blocking was removed and primary antibodies were added. Then the streptavidin-biotin-peroxidase complex (GE Healthcare, Buckinghamshire, UK) was placed on the sections. Subsequently, the staining

was visualized by using 3-amino-9-ethylcarbazole (AEC [Sigma Aldrich Chemie, Zwijndrecht, The Netherlands]), and counter staining with Haematoxylin (Klinipath B.V., Duiven, The Netherlands). The slides were sealed with Kaiser's glycerine (BOOM B.V., Meppel, The Netherlands). Microscopic images were taken with a light microscope (Zeiss Axioplan 2, Zeiss, The Netherlands). The proliferation index was calculated for Ki67 using the following method. A minimum of 100 cells at the basal layer were counted for four sections of each slide and the stained nuclei were divided by the total number of counted cells (e.g., 12 stained from a total of 100 means 12% proliferation index). This was performed FTM of 3 donors.

Table S1: immunohistochemistry antibody list and specific methods

Immunohistochemistry	Origin	Clone	Dilution	Antigen Retrieval	Secondary antibody	Manufacturer
Primary antibody						
Ki67	Mouse	MIB1	1:100	AC	A	Dako, Denmark
Cytokeratin 10	Mouse	DE-K10	1:50	AC	A	Labvision/ Neomakers, USA
Involucrin	Mouse	SY5	1:1200	AC	A	Sanbio, The Netherlands
Stearoyl-CoA desaturase	Mouse	CD.E10	1:300	WB	A	Abcan, Cambridge, UK
Secondary antibody						
Biotinylated Goat anti-mouse (A)	Goat		1:200			Southern Biotechnology

AC- autoclave; WB - water bath

1.4. Liquid chromatography - mass spectrometry (LC-MS)

1.4.1. Lipid extraction

Extraction of the SC lipids was performed using an adapted Blight and Dyer method. This method has been described elsewhere [2]. After the extraction, the samples were stored in a glass vial under argon at 4°C until CER and FFA analysis was performed. For NHS, the SC originated from 3 Caucasian female skin donors aged 18-26. Furthermore, for each of the CER or FFA runs, a Quality Control sample that consisted out of multiple NHS samples pooled together was added to ensure reproducibility between and during the run.

1.4.2. CER analysis

CER analysis was performed as reported elsewhere [3]. In short, the solvent in the samples was evaporated and reconstituted in 95:21/2:21/2 (v/v/v) heptane:chloroform:methanol to a concentration of 0.3 mg/ml. An injection standard, deuterated CER[NS] (C24deuterated; C18 protonated, Evonik Industries, Essen, Germany for abbreviations see Fig S2), was added. From the reconstituted sample, 5 μ l was injected into the UPLC. The UPLC-MS setup consisted of an Acquity UPLC H-class (Waters, Milford, MA, USA) coupled to an XEVO TQ-S mass spectrometer (waters, Milford, MA, USA) with an atmospheric pressure chemical ionization (APCI) chamber. Detection occurred in full scan m/z between 350 and 1200 atmospheric mass units (amu) in positive ion mode. Separation of CERs was performed on a PVA-Sil column (5 μ m particles size, 100x2.1 mm i.d., YMC, Kyoto, Japan) as described in detail before [2]. Data analysis was performed by Waters Masslynx 4.1 and area under the curve (AUC) was used for the detection of the CER species. 15 CER subclasses were analyzed. For the CER class containing [N] non-hydroxy and [A] α -hydroxy (belonging to the CER[non-EO]), the subclasses [NdS], [NS], [NP], [NH], [AdS], [AS], [AP], and [AH] were quantified. For the CER class containing the linoleic acid esterified to an ω -hydroxy (belonging to the CER[EO]), the subclasses [EOdS], [EOS], [EOP], and [EOH] were analyzed. For the CER class containing the ω -hydroxy (CER[O]) the subclasses [OS], [OP], and [OH] were examined. The subclasses classification and abbreviations are explained in Fig S2. The abbreviations are according to Motta et al [4]. AUCs were corrected according to the processing method [2]. After data corrections, areas were converted to nmol and plotted in absolute values (CER nmol / mg SC) or CER mol (%).

1.4.3. FFA analysis

Samples were evaporated under a gentle stream of nitrogen and reconstituted in isopropanol to a concentration of 0.75 mg/ml. After adding the deuterated C24 (C24D47) internal standard (purchased at Sigma-Aldrich Zwijndrecht, The Netherlands), 2 μ l was injected into a UPLC. UPLC-MS setup consisted of a Waters Acquity UPLC H-class system (Waters, Milford, MA, USA) coupled to a XEVO TQ-S mass spectrometer (waters, Milford, MA, USA) connected to an atmospheric pressure chemical ionization (APCI) chamber (probe temperature: 425°C, discharge current 3 μ A). Detection occurred in negative ion mode measuring full scan m/z between 200 and 550 amu. FFAs were separated using a Purospher Star LiChroCART reverse phase column (3 μ m particle size, 55x2 mm i.d., Merck, Darmstadt, Germany) between 0-6 min with a flow rate of 0.5 ml/min. The gradient started at acetonitrile/water/chloroform/acetic acid (90:10:2:0.005(v/v/v/v)) and shifted to methanol/heptane/chloroform/acetic acid (90:10:2:0.005). Data analysis was performed by Waters Masslynx 4.1 and the area under the curve (AUC) was calculated. FFA analysis included the following: monounsaturated FFA: (C20:1, C22:1, and C24:1) and saturated FFAs: (C20, C22, C23, C24, C25, C26, C28, and C30). As chloroform was manufacturer contaminated with FFA C16 and C18, these FFA could

not be determined accurately and were therefore excluded in the analysis.

Subsequently the AUCs were corrected for the internal standard (C24D47) and corrected for response using FFA standards calibration curves for: C20:0, C20:1, C22:0, C22:1, C23:0, C24:0, C24:1, C25:0, C26:0, C28:0, and C30:0 (Sigma-Aldrich, Zwijndrecht, The Netherlands).

1.5. qPCR

Isolation of RNA was performed with the Favorprep Tissue total RNA mini kit (Bio-connect BV, Huissen, The Netherlands). The concentration and purity of the RNA was determined with the NanoDrop One (Thermo Scientific). cDNA was synthesized using C1000 touch thermal cycler (Biorad). The cDNA mixture contained 4 μ L of 5x iScript reaction mix, 1 μ L iScript reverse transcriptase, and 500 ng cDNA in 15 μ L RNA-free H₂O. The run was performed by a CFX384 real time system (Biorad) and each well contained 3.5 μ L SYBR green, 2.275 μ L RNA-free H₂O, 0.875 cDNA, and 0.35 μ L of Primer work solution (10 μ M forward and reverse primer in RNA-free H₂O). The following primers were used: SREBP-1c, ACC1, FAS, ELOVL1, ELOVL4, SCD-1, ABCA1, CerS2, CerS3, CerS4, CerS5, CerS6, DES1, and DES2. The forward and reverse sequence of these primers are listed in table 2.

Table S2: primer and housekeeping sequences.

SREBP1c_F	GGAGGGGTAGGGCCAACGGCCT	DES1_F	TCCCAACATTCTGGAAAAAG
SREBP1c_R	CATGCTTCGAAAAGTCAATCC	DES1_R	CAGGAATTGTAGTGAGGGAGGT
ACC1_F	CATATCCAGTCCATGCTGCGT	DES2_F	GCATCCCGGGCTACAACCT
ACC1_R	GTCCAGCCACTGCACAACC	DES2_R	CCAGGGAGTCCCTCAACACAA
FASN_F2	CATCCCCACCTATGGCCTGC		
FASN_R2	GCCTGATGCAGTCGATGTAGTA	Housekeeping gene	Sequence
ELOVL1_F1	GGCTCTTCTCTTCTCCAAGTT	SDHA_F	AACCAACCGCTGGGGAAGAA
ELOVL1_R1	TCCAGGGAAGCACAGAGTGAT	SDHA_R	GGAACACGGCAGCATGATT
ELOVL4_F	TTTGGTGVAAACGATACCTGA	ZNF410_F	GCTGTGGTAAGCAGTTTACTACAG
ELOVL4_R	TTAGAGCCCAGTGCATCCAT	ZNF410_R	CTTGGGCTTCACAAGGAAAGG
SCD-1_F	ACAGTGCTGCCACCTCTTCG	ARCP2_F	TCCGGGACTACCTGCCTACTAC
SCD-1_R	CCCTCACCCACAGCTCCAAGTG	ARCP2_R	GGTTCAGCACCTTGAGGAAG
ABCA1_F	TGGCTCTCTAATTTTGTCTGGGA		
ABCA1_R	TAGCACAGGCAGATTGGTGG		
CERS2_F	CTTCATCGTCTCGCCATTGTT		
CERS2_R	AGGATAGAGCTCCAGTGGGTA		
CERS3_F	CCCTGTTTTTCATCTTCCACC		
CERS3_R	TAGGCAAGATCAGCGTGCAA		
CERS4_F	GTGCTGCTGTACACGATTCC		
CERS4_R	GTCGCACACTTGCTGATACTG		
CERS5_F	CGGCTCTGTGACACCCCTT		
CERS5_R	TCTCAAAGAGGGTCTGTGTTCA		
CERS6_F	TGTTGTTATGTTTGCCGTGGT		
CERS6_R	CCAACGATCTCCAGCTTCA		

1.6. Small angle X-ray diffraction (SAXD) analysis

X-ray diffraction studies were performed at BM26B at the European Synchrotron Radiation Facility (ESRF, Grenoble, France). The setup of this analysis is described elsewhere [5]. Prior to measurement, isolated SC sheets were equilibrated for 24 hours in a humidity chamber

at room temperature using 27% NaBr solution (w/v). The Pilatus 1M detector was calibrated using AgBr and cholesterol. Measurements were performed at room temperature (24°C) in 2x90 sec and dual imaged were merged in the sample processing. The distance between the sample and detector was 2.1 m. After acquiring the scattering profile, the 2D images were converted to a 1D image by converting the Cartesian (x,y) to polar (r,θ) coordinates by integrating over θ. A diffraction pattern attributed to a lamellar phase is characterised by diffraction peaks at equidistant position from each other. From the position of these peaks the repeat distance or spacing (d) is calculated by $d = 2n\pi/q$. In this formula, the scattering vector $q = 4\pi \sin \theta/\lambda$, where θ is the scattering angle, and λ, the X-ray wavelength, was 0.1033 nm.

1.7. Fourier transformed infrared spectroscopy (FTIR analysis)

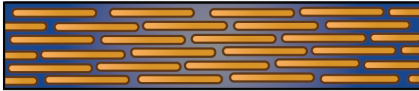
FTIR measurements were performed on a Varian 670-IR spectrometer (Varian Inc., Santa Clara, CA) equipped with a broad band Mercury-Cadmium-Telluride (MCT) detector. This method is described elsewhere [6]. Before the measurement, SC was hydrated for 24 hours in a humidity chamber containing deuterated water. After hydration, the SC was placed between two AgBr windows and was subsequently heated to 24°C. The temperature gradient was 0.25°C/min and spectra were collected with 2 cm⁻¹ resolution. In the acquired spectra, the rocking area (710-740 cm⁻¹) was analyzed by the Varian Resolution Pro software (v4.1).

1.8. Transepidermal water loss (TEWL)

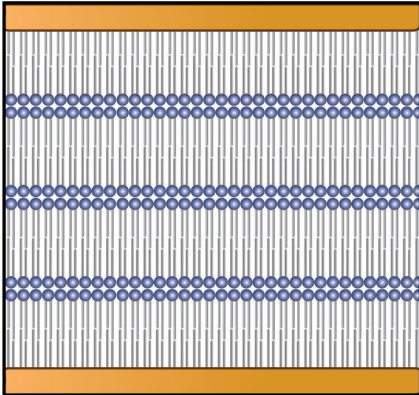
Trans epidermal water loss (TEWL) was measured using isolated SC from NHS and the FTMs. The SC was placed on a polycarbonate filter (Diachema, Munich, Germany) and mounted in a PermeGear inline diffusion cell (Bethlehem, PA, USA). The donor compartment was empty and the acceptor compartment was filled with milliQ water to hydrate the sample. After 15 min hydration, the TEWL was measured by an evaporimeter (Aqua Flux AF200, Biox Systems Ltd, London, UK) connected to a modified nozzle to close the donor compartment. Measurements were performed each 10 sec for a period of 15 min. The data points used in the graph are the average of the final three min (28-30 min) when the TEWL was stabilized.

Corneocytes and lipid matrix

(a) Brick and mortar structure

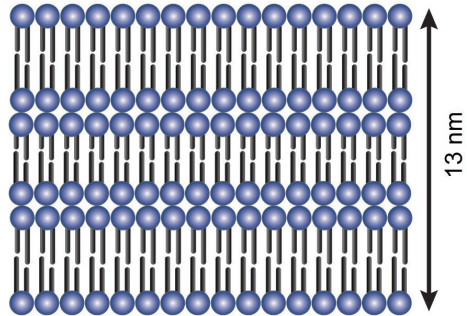


(b) Corneocytes and lipid matrix

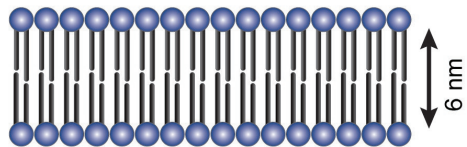


Lipid matrix

(c) Long periodicity phase



(d) Short periodicity phase



Lateral lipid organization

(e) different organizations of the acyl-chains

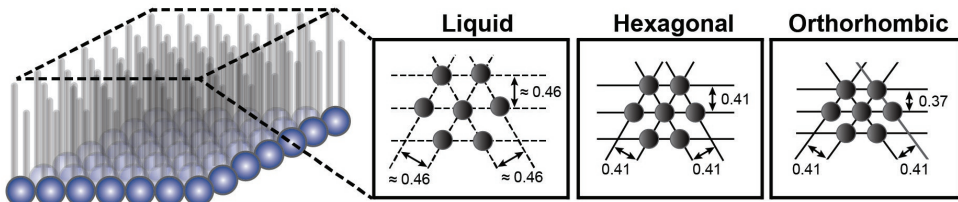


Fig S1: Schematic presentation of the organization in the lipid matrix between corneocytes. (a) The SC is organized in a brick and mortar structure, (b) between the corneocytes lipid lamellae are present. Two different lamellar phases are identified, the long periodicity phase (LPP) depicted in (c), and the short periodicity phase (SPP) depicted in (d). The hydrocarbon chains can assemble in different types of packing referred to as the lateral organization (e), which is either liquid (loose packing), hexagonal (dense packing) or orthorhombic (very dense packing).

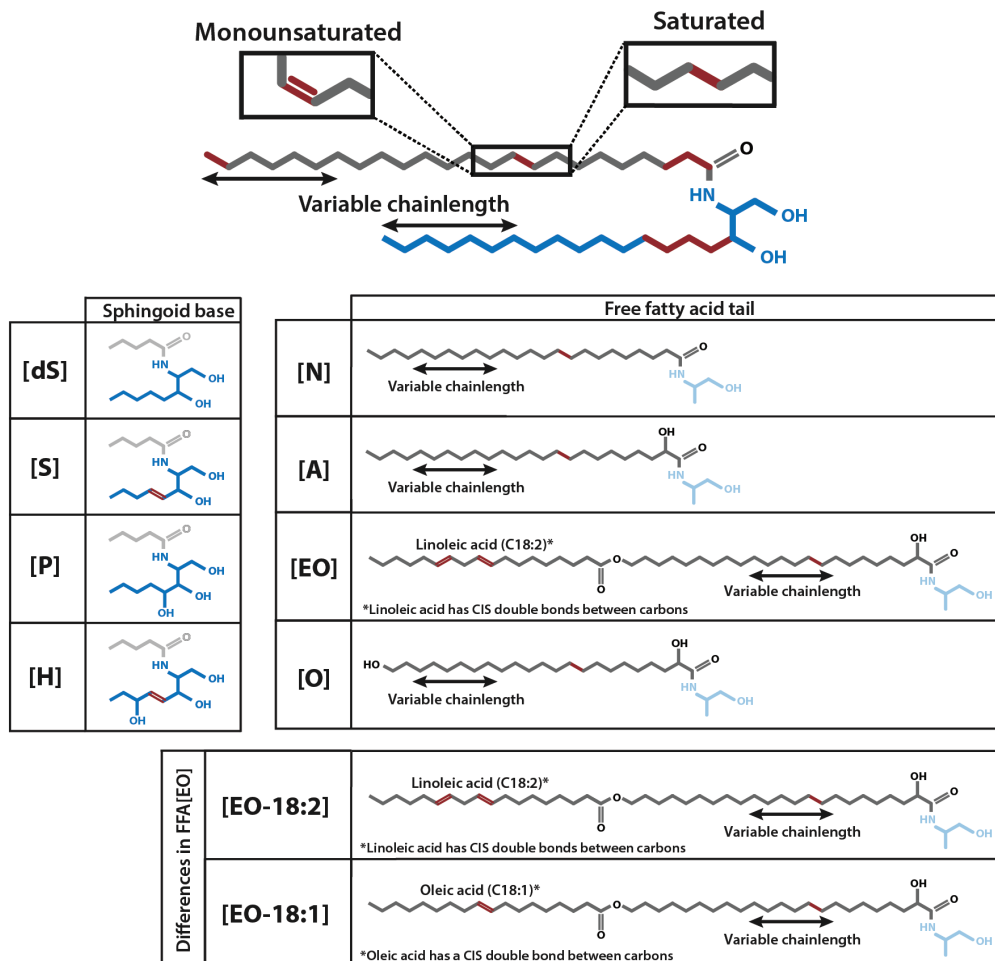


Fig S2: Molecular structure of the CER subclasses. The 16 CER subclasses that were analyzed are shown in the ion map. CERs consist of an acyl tail: [N] non-hydroxy, [A] α -hydroxy, [EO] linoleic acid esterified to an ω -hydroxy or [O] ω -hydroxy. The acyl-chain is linked to a sphingoid base: [dS] dihydrosphingosine, [S] sphingosine, [P] phytosphingosine or [H] 6-hydroxysphingosine. There are three CER classes i) CER[non-EO] with subclasses [NdS], [NS], [NP], [NH], [AdS], [AS], [AP], and [AH], ii) CER[EO] with subclasses [EOdS], [EOS], [EOP], and [EOH] and iii) CER[O] with subclasses [OS], [OP], and [OH]. In each subclass, CERs vary in chain length and can be either saturated or monounsaturated. In addition, CER[EO] structure containing an esterified-oleic acid rather than linoleic acid is also shown.

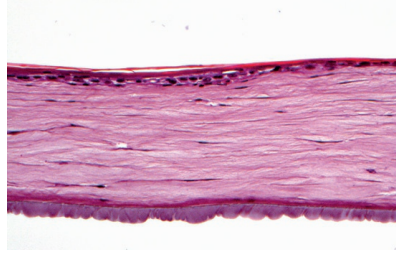


Fig S3: High concentrations of SCD-1 antagonist prevented the formation of a viable epidermis. H&E staining of the FTM cultured with 450 nM concentration did not result in a viable epidermis.

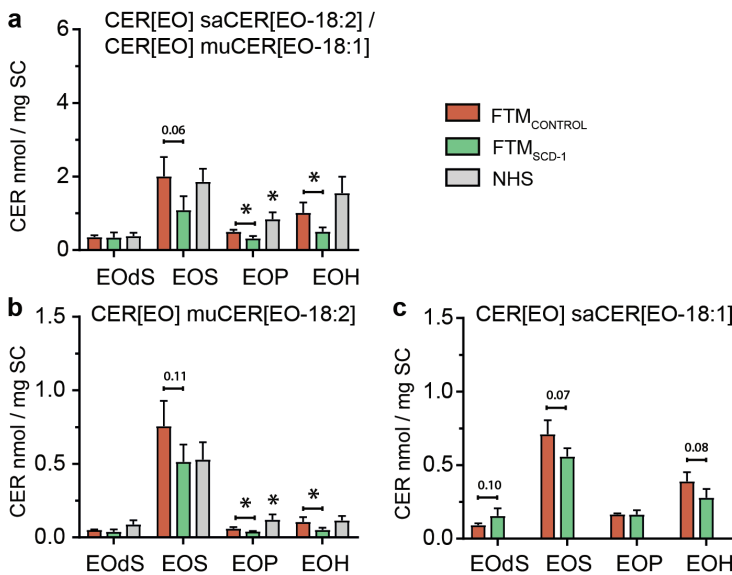


Fig S4: SCD-1 inhibition led to a reduction in the level of CER[EOS] in the FTMs. The profile of the absolute amount of the subclasses of CER[EO] was determined for NHS, FTM_{CONTROL} and FTM_{SCD-1}; (a) Amount of subclasses of muCER[EO-18:2]; (b) Amount of subclasses of muCER[EO-18:1]/saCER[EO-18:2]; (c) amount of subclasses of saCER[EO-18:1]. For statistical analysis, an unpaired t-test was performed between the FTM_{CONTROL} and FTM_{SCD-1}. The amounts of muCER[EO-18:1]/saCER[EO-18:2] cannot be separately determined in the LC/MS method employed and are therefore grouped together. To compare the FTM_{CONTROL} vs NHS, an unpaired t-test was used. Significant differences are indicated by * for p<0.05.

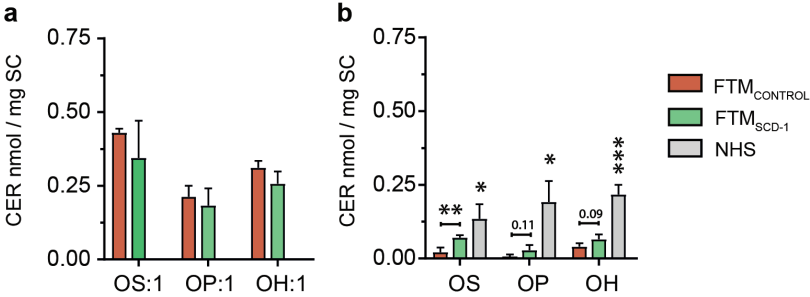


Fig S5: SCD-1 inhibition led an increased level of saCER[O] in the FTMs. The absolute CER[O] profile was calculated for NHS, FTM_{CONTROL} and FTM_{SCD-1}; (a) Amount of all muCER[O] subclasses; (b) Amount of saCER[O] subclasses. For statistical analysis, an unpaired t-test was performed between the FTM_{CONTROL} and FTM_{SCD-1}. To compare the FTM_{CONTROL} vs NHS, an unpaired t-test was used. Significant differences are indicated by * for p<0.05, ** for p<0.01, and *** for p<0.001.

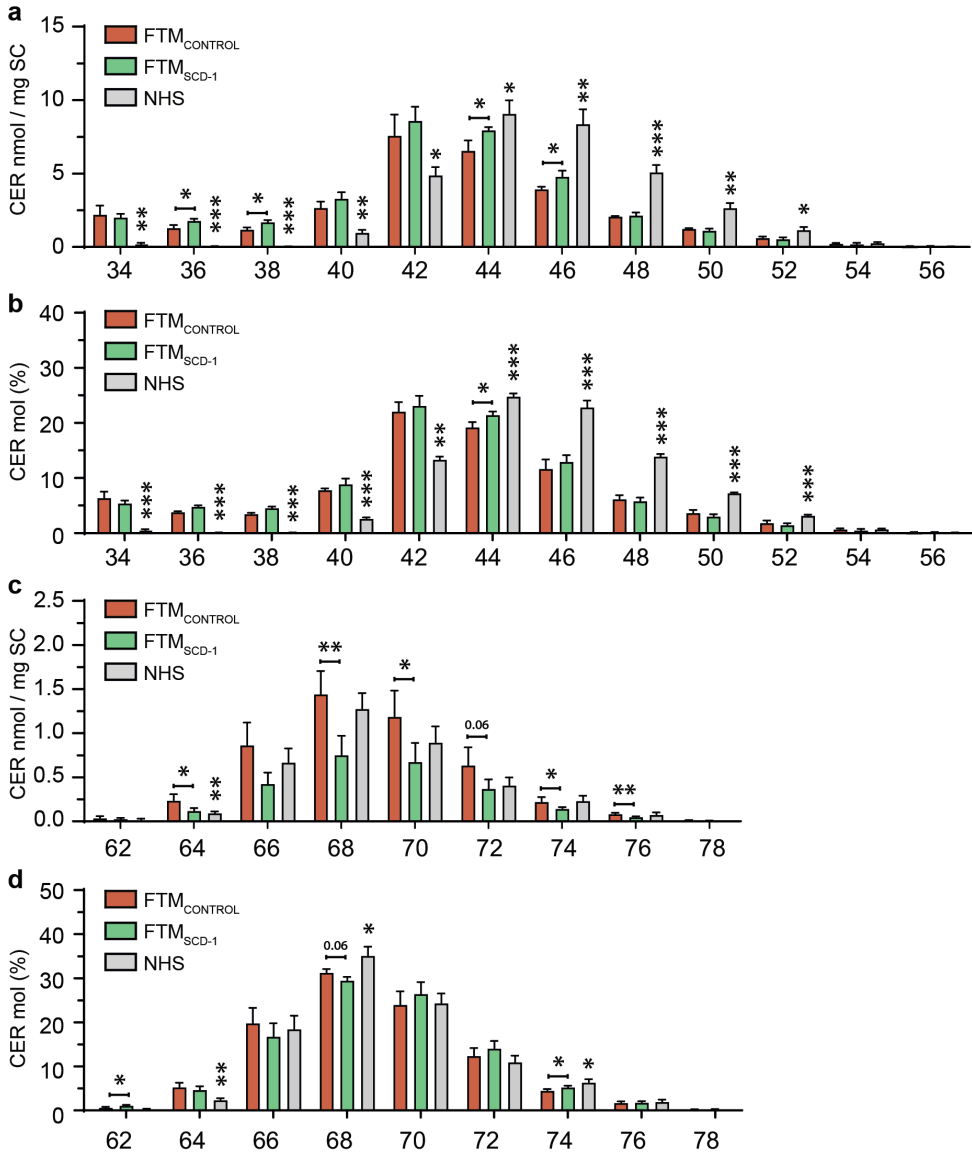


Fig S6: Inhibition of SCD-1 led to similar chain length distribution. The chain length profile of CER[non-EO] were calculated in (a) absolute amounts and (b) relative amounts. This was also done for CER[EO] in (c) absolute amounts and (d) in relative amounts. For statistical analysis, an unpaired t-test was performed between the FTM_{CONTROL} and FTM_{SCD-1}. To compare the FTM_{CONTROL} vs NHS, an unpaired t-test was used. Significant differences are indicated by * for p<0.05, ** for p<0.01, and *** for p<0.001.

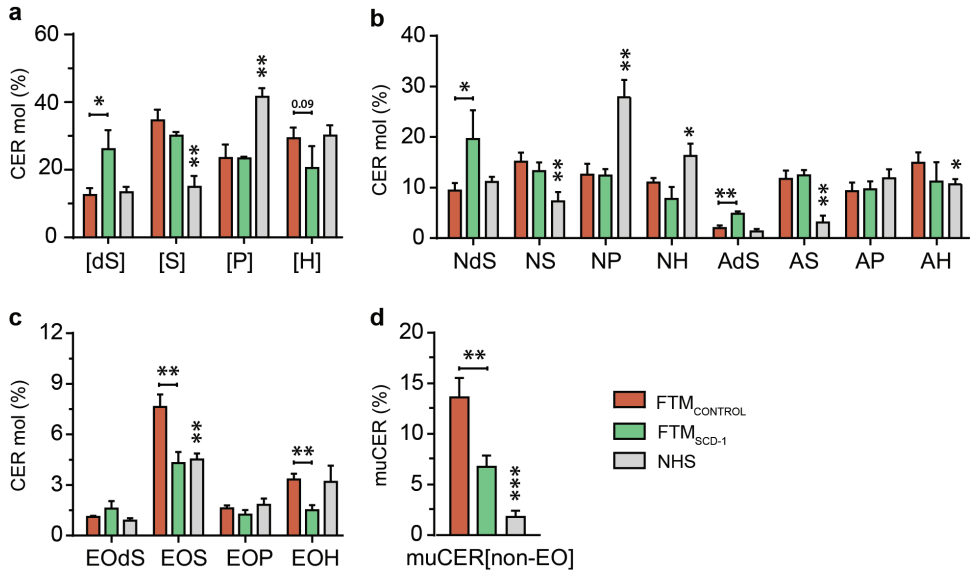


Fig S7: SCD-1 inhibition alters lipid composition by reducing the monounsaturations, reducing the CER[EO] subclasses, and by increasing the CER[dS] fraction. (a) The percentage of the CER[non-EO] head groups (saCER+muCER); (b) The percentage amount of individual CER[non-EO] subclasses (saCER+muCER); (c) Percentage of the CER[EO] subclasses (saCER+muCER); (d) The total percentage of muCER[non-EO] subclasses compared to the total amount of CER[non-EO]. For statistical analysis, an unpaired t-test was performed between the FTM_{CONTROL} and FTM_{SCD-1}. After, to compare the FTM_{CONTROL} and NHS, an unpaired t-test was used. Significant differences are indicated by * for $p < 0.05$, ** for $p < 0.01$, and *** for $p < 0.001$.

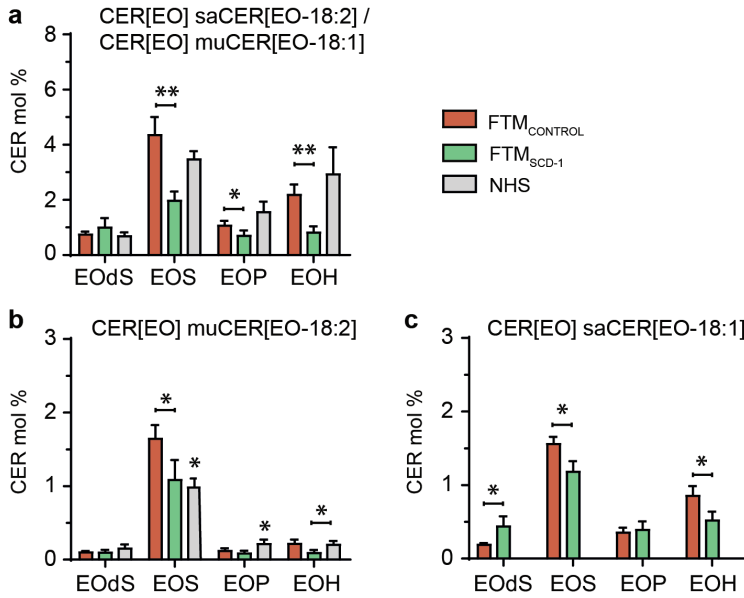


Fig S8: SCD-1 inhibition led to a strong reduction in the level of CER[EOS] in the FTMs. The relative CER[EO] profile for NHS and FTM_{CONTROL} and FTM_{SCD-1} (a) percentage of all CER[EO] subclasses and compositions; (b) Percentage of muCER[EO-18:2] subclasses; (c) Percentage of muCER[EO-18:1] / saCER[EO-18:2] subclasses; (d) Percentage of saCER[EO-18:1] subclasses. For statistical analysis, an unpaired t-test was performed between the FTM_{CONTROL} and FTM_{SCD-1}. To compare the FTM_{CONTROL} vs NHS, an unpaired t-test was used. Significant differences are indicated by * for p<0.05 and ** for p<0.01.

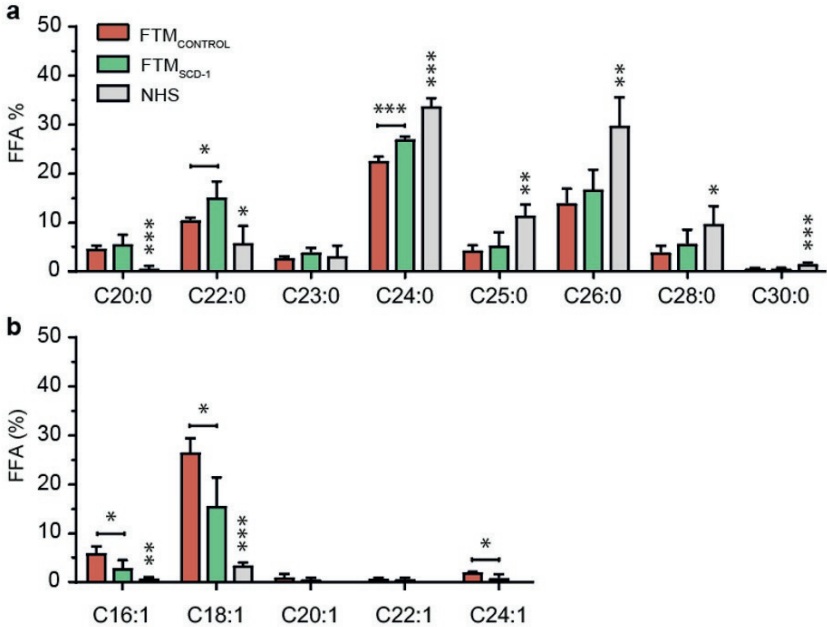


Fig S9: FFA composition after SCD-1 inhibition reduced the level of muFFAs. (a) Relative saFFA chain length distribution. (b) Relative muFFA chain length distribution. (d) For statistical analysis, an unpaired t-test was performed between the FTM_{CONTROL} and FTM_{SCD-1}. To compare the FTM_{CONTROL} vs NHS, an unpaired t-test was used. Significant differences are indicated by * for p<0.05 and ** for p<0.01.

Supplementary References

1. Thakoersing, V.S., Gooris, G.S., Mulder, A.A., Rietveld, M., El Ghalbzouri, A., andBouwstra, J.A. Unraveling barrier properties of three different in-house human skin equivalents. *Tissue Eng Part C Methods* 18, 1, 2012.
2. Boiten, W.A., Absalah, S., Vreeken, R.J., Bouwstra, J.A., andvan Smeden, J. Quantitative analysis of ceramides using a novel lipidomics approach with three dimensional response modelling. *Biochim Biophys Acta* 1861, 1652, 2016.
3. Boiten, W., Absalah, S., Vreeken, R., Bouwstra, J., andvan Smeden, J. Quantitative analysis of ceramides using a novel lipidomics approach with three dimensional response modelling. *Biochimica et Biophysica Acta (BBA) - Molecular and Cell Biology of Lipids* 1861, 1652, 2016.
4. Motta, S., Monti, M., Sesana, S., Caputo, R., Carelli, S., andGhidoni, R. Ceramide composition of the psoriatic scale. *Biochim Biophys Acta* 1182, 147, 1993.
5. Mojumdar, E.H., Helder, R.W.J., Gooris, G.S., andBouwstra, J.A. Monounsaturated Fatty Acids Reduce the Barrier of Stratum Corneum Lipid Membranes by Enhancing the Formation of a Hexagonal Lateral Packing. *Langmuir* 30, 6534, 2014.
6. Janssens, M., van Smeden, J., Gooris, G.S., Bras, W., Portale, G., Caspers, P.J., et al. Increase in short-chain ceramides correlates with an altered lipid organization and decreased barrier function in atopic eczema patients. *Journal of lipid research* 53, 2755, 2012.